Electronic Supporting Information

Spin density localization and accessibility of organic radicals affect liquid-state DNP efficiency

M. Levien[a,b], M. Reinhard[a,b], M. Hiller[a], I. Tkach[a], M. Bennati[a,b], T. Orlando[a]

[a]*Research Group EPR Spectroscopy, Max Planck Institute for Biophysical Chemistry, Göttingen, Germany*
[b]*Department of Chemistry, Georg-August University, Göttingen, Germany*

Contents

S1   Sample preparation

Organic radicals α, γ-Bisdiphenylene-β-phenylallyl (BDPA, 1:1 complex with benzene), Di-*tert*-butyl-nitroxide (DTBN), 4-Hydroxy-2,2,6,6-tetramethylpiperidine 1-oxyl or Tempol (TL) and 4-Oxo-2,2,6,6-tetramethylpiperidine-d$_{16}$,1-^{15}N-1-oxyl or Tempone (TN) were purchased from Sigma-Aldrich and used as received. 7-Aza-3,11-dioxa-15-oxodispiro[5.1.5.3]hexadec-7-yl-7-oxyl (TN-py) was prepared in house according to a protocol from Ref. [1].

^{13}CCl$_4$ and ^{13}CHCl$_3$ were purchased from Eurisotop and Sigma-Aldrich, respectively. As the pH value of ^{13}CHCl$_3$ was ~ 1 upon delivery, K$_2$CO$_3$ was added until a pH of $6-7$ was reached. Roughly 1% ethanol (of the absolute volume of ^{13}CHCl$_3$) was added for stabilization. Unlabelled tetrachloromethane, chloroform and toluene were purchased from Merck KGaA and Sigma-Aldrich.

PA concentrations range between $1\,\mathrm{mM}$ and $16\,\mathrm{mM}$ and were verified by continuous wave (cw) measurements. Approximately $7\,\mu\mathrm{L}$ per sample were inserted in a quartz tube with an outer diameter of $1.6\,\mathrm{mm}$ and an inner diameter of $1.1\,\mathrm{mm}$. All samples were degassed by freeze-pump-thaw cycles (from two to four) to remove dissolved oxygen. Degassing small amounts of sample results in an error of up to 15% for the concentration.

S2   Overhauser experiments and parameters

^{1}H-DNP at X-Band $-$ 0.34 T

Measurements were performed using a Bruker ElexSys E580 EPR spectrometer combined with an AVANCE III ^{1}H 300 MHz NMR console. We utilized an EN 4118X-MD-4 EPR resonator with Electron Nuclear Double Resonance (ENDOR) capabilities. The ENDOR coil was used to excite and detect the NMR transitions. EPR and ELDOR measurements (see below) were performed employing a 1 kW TWT microwave amplifier, while for DNP measurements we utilized a AmpX 5 W cw mw amplifier. Comparability of the results was demonstrated before [2].

^{1}H NMR signal enhancements were obtained from comparison of the integrated NMR signal with and without mircowave. Boltzmann signals were typically acquired using up to 64 scans, while 1 or 2 scans

Table S1: ^{1}H Overhauser parameter of the methyl group of toluene for different PAs at room temperature and at 0.34 T. The leakage factor f was calculated using $T_{1n}^0 = 8.1$ s (ref. [5]). Errors of the concentration are $10-15\%$, for T_{1n}, $T_{\text{Build-up}}$, s, ϵ and f 10% and for ξ 15%. As $T_{1n} \neq T_{\text{Build-up}}$ for DTBN, errors for ϵ and ξ are increased to 15 and 25 %, respectively (see error discussion in SI sec. S2). (*) Data from ref. [5].

^{1}H-DNP in toluene - methyl protons

	c (mM)	T_{1n} (s)	$T_{\text{Build-up}}$ (s)	f	s_{eff}	ϵ	ξ
DTBN	2	4.9	3.8	0.40	0.58	-62	0.42
^{15}N-TN	2	3.8	3.4	0.53	0.78	-88	0.33
TL*	1.5	4.7	4.7	0.42	0.58	-45	0.28
TN-py	2	2.6	2.6	0.68	0.80	-86	0.24
BDPA	2	4.2	4.8	0.48	1.00	-45	0.14

were recorded under DNP conditions. The used recycle delay was $\sim 5 \times T_{1n}$. The signal enhancement can be calculated:

$$\epsilon = \frac{I_{\text{DNP}}}{I_{\text{Bltz}}} \cdot \frac{n_{\text{Bltz}}}{n_{\text{DNP}}}, \tag{S1}$$

where $I_{\text{DNP/Bltz}}$ is the integral of the NMR signal with and without mw irradiation and $n_{\text{DNP/Bltz}}$ is the number of scans with and without mw irradiation. Figure S1a shows the enhanced NMR signal and the Boltzmann signal of toluene doped with DTBN.

Saturation factors were determined using an ELDOR (Electron Nuclear Double Resonance) sequence. During this experiments, EPR detection is performed on one of the EPR lines while a long saturation pulse $(3-5\,\mu\text{s})$ is swept through the EPR spectrum. At positions where the ELDOR pulse is on resonance with either one of the lines, a signal drop is detected. From these intensity drops the saturation factor of each line can be obtained. The effective saturation factor s_{eff} for a n-line systems is calculated as follows: [3,4]

$$s_{\text{eff}} = \frac{1}{n} \cdot \sum_{i=1}^{n} s_i. \tag{S2}$$

Figure S1b shows the ELDOR curve for DTBN in toluene and, in the inset, the ELDOR pulse sequence.

The leakage factor f can be calculated with the formula:

$$f = 1 - \frac{T_{1n}}{T_{1n}^0}, \tag{S3}$$

where T_{1n} and T_{1n}^0 are the nuclear relaxation times in presence and absence of paramagnetic substance. T_{1n} was measured with a saturation recovery experiment (8 saturation pulses with a duration of 6 µs each, $(\pi/2)_{\text{RF}} = 6\,\mu\text{s}$, $P_{\text{RF}} = 60\,\text{W}$). Build-up times $T_{\text{Build-up}}$ were measured by increasing the mw irradiation time. Both T_{1n} and $T_{\text{Build-up}}$ were obtained from fitting the experimental data to a mono exponential function i.e. $y = A(1 - \exp(-t/T_i))$. Examples of T_{1n} and $T_{\text{Build-up}}$ recoveries are shown in Figures S1c and S1d, together with the respective pulse sequences.

The experimental results of ^{1}H-DNP measurements at 0.34 T for different PAs and solvents are summarised in Tab. S1-S3, Figure S3, and Figure S2.
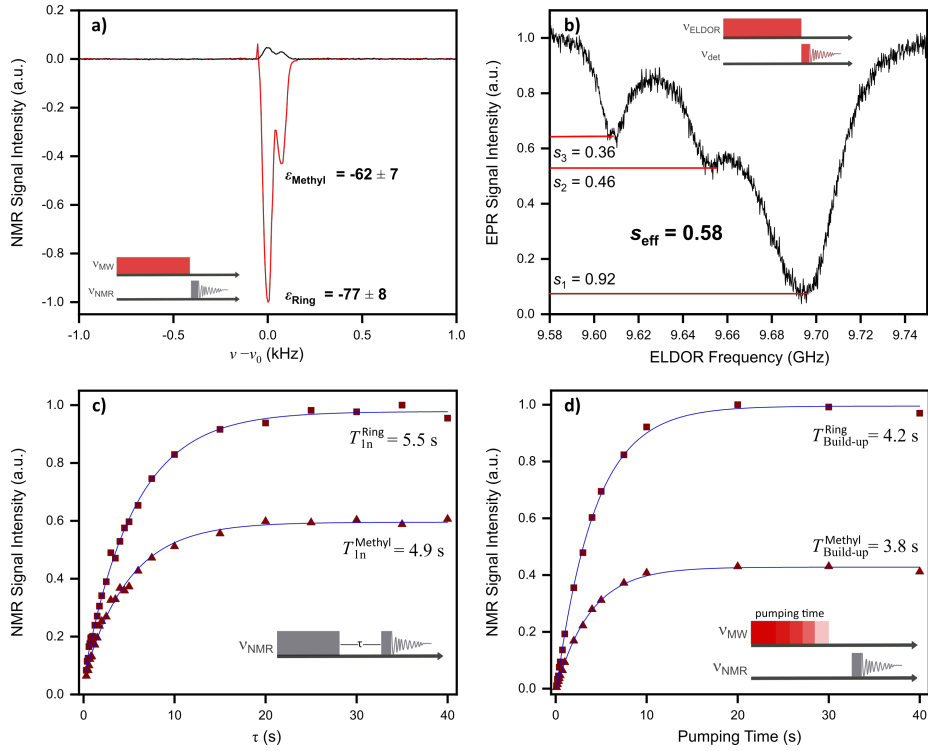
Figure S1: a) ^{1}H NMR signal with (red) and without (black) mw irradiation of toluene using DTBN as a PA. b) saturation curve (black) of DTBN in toluene, s_{eff} results as the average of s_1, s_2 and s_3. c) T_{1n} determination via saturation recovery measurements; d) measurement of $T_{Build-up}$ by increasing the mw pumping time (red squares for the ring protons and red triangles for the methyl group of toluene) at $0.34\,T$. Blue curves are the mono exponential fits used to obtain T_{1n} and $T_{Build-up}$.

Table S2: ^{1}H Overhauser parameter of the ring protons of toluene for different PAs at room temperature and at $0.34\,T$. The leakage factor f was calculated using $T_{1n}^0 = 12.5\,s$ (ref. [5]). Errors of the concentration are $10 - 15\,\%$, for T_{1n}, $T_{Build-up}$, s, ϵ and f $10\,\%$ and for ξ $15\,\%$. As $T_{1n} \neq T_{Build-up}$ for DTBN, errors for ϵ and ξ are increased to 15 and $25\,\%$, respectively (see error discussion in SI sec. S2). (*) Data from ref. [5].

^{1}H-DNP in toluene - aromatic protons

	$c\,(mM)$	$T_{1n}\,(s)$	$T_{Build-up}\,(s)$	f	s_{eff}	ϵ	ξ
DTBN	2	5.5	4.2	0.56	0.58	-77	0.36
^{15}N-TN	2	4.2	3.6	0.67	0.78	-108	0.32
TL*	1.5	5.5	5.5	0.56	0.58	-61	0.29
TN-py	2	2.6	2.7	0.79	0.80	-109	0.26
BDPA	2	5.2	6.3	0.58	1.00	-63	0.17

Table S3: ^{1}H Overhauser parameter of chloroform for different PAs at room temperature and at $0.34\,T$. The leakage factor f was calculated using $T_{1n}^0 = 82.5\,s$ (ref. [5]). Errors of the concentration are $10-15\,\%$, for T_{1n}, $T_{Build-up}$, s, ϵ and f $10\,\%$ and for ξ $15\,\%$. As $T_{1n} \neq T_{Build-up}$ for DTBN, TN-py and TN errors for ϵ and ξ are increased to 15 and $25\,\%$, respectively (see error discussion in SI sec. S2). (*) Data from ref. [5].

^{1}H-DNP in CHCl$_3$

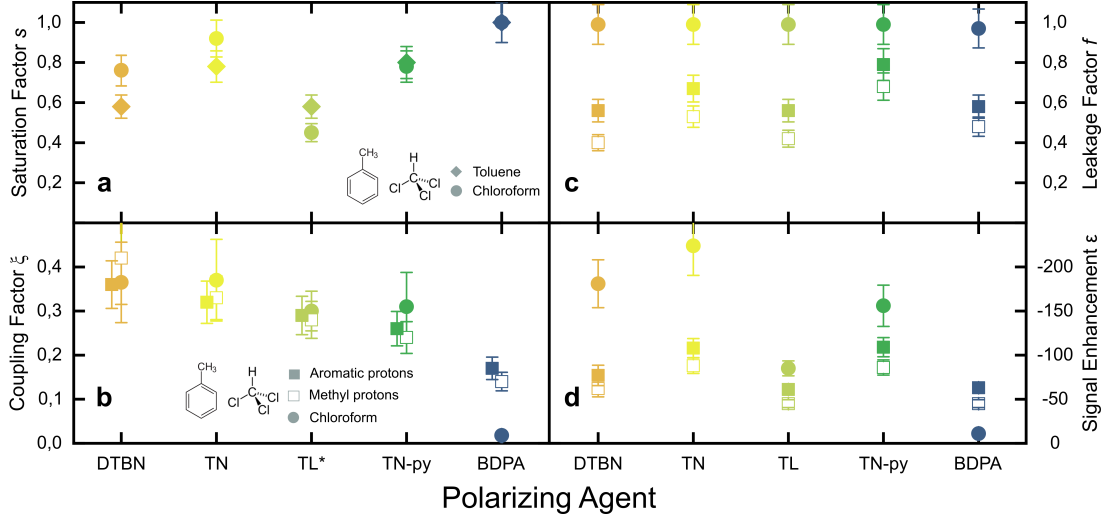|	$c\,(mM)$	$T_{1n}\,(s)$	$T_{Build-up}\,(s)$	f	s_{eff}	ϵ	ξ
DTBN	10	0.73	0.51	0.99	0.72	-163	0.35
DTBN	16	0.12	0.10	0.99	0.79	-199	0.38
^{15}N-TN	10	0.32	0.21	0.99	0.92	-224	0.37
TL*	0.5	2.8	2.9	0.97	0.45	-85	0.30
TN-py	10	0.42	0.24	0.99	0.78	-156	0.31
BDPA	10	0.56	0.69	0.99	1.00	-11	0.018

Figure S2: Plots of the ^{1}H-DNP Overhauser parameters from Tables S1, S2, S3.

Table S4: ^{13}C Overhauser parameter of ^{13}CCl$_4$ for different PAs at room temperature and at 1.2 T. The leakage factor f was calculated using $T_{1n}^0 = 200\,\mathrm{s}$. [6] Errors of the concentration are $10 - 15\,\%$, for T_{1n}, $T_{\mathrm{Build\text{-}up}}$, s, ϵ and f 10 % and for ξ 15 %. As $T_{1n} \neq T_{\mathrm{Build\text{-}up}}$ for TN-py and BDPA errors for ϵ and ξ are increased to 15 and 25 %, respectively (see error discussion in SI sec. S2). (*) Data from ref. [5].

^{13}C-DNP in CCl$_4$

	c (mM)	T_{1n} (s)	$T_{\mathrm{Build\text{-}up}}$ (s)	f	s_{eff}	ϵ	ξ
BDPA	10	47.0	33.0	0.84	0.95	98	-0.047
TN-py	10	9.3	6.7	0.95	0.06	22	-0.14
DTBN	10	6.7	6.1	0.97	0.05	41	-0.32
TL	10	7.7	6.8	0.96	0.11	75	-0.27
^{15}N-TN*	10	18.5	16.6	0.93	0.25	250	-0.41
TP-CLST*	10	2.9	3.4	0.99	0.12	150	-0.48
FN2a*	10	3.8	3.8	0.98	0.33	550	-0.65

^{13}C-DNP at Q-Band − 1.2 T

^{13}C-DNP at 1.2 T was performed on an Bruker ElexSys E580 EPR spectrometer combined with an AVANCE III ^{1}H 300 MHz NMR console. We used a Bruker ER-5106QT/W cw resonator. For NMR detection, a copper coil was wrapped around the tube, thereby reducing the Q-value of the resonator. In order to limit sample heating during mw irradiation, we operated at low mw power (< 3 W).

The parameters s, f, and ϵ were measured as described in the previous section. However, due to the low NMR sensitivity, T_{1n} was measured with a pre-polarization sequence, where a short mw pulse (< 3 s) is introduced before the $\pi/2$ NMR detection. The time t between the two pulses is incremented, and the signal decay is fitted to the exponential function $A \cdot \exp\left(-t/T_{1n}\right)$. During the measurement of the saturation factor of BDPA in ^{13}CHCl$_3$ we observed an artefact which led to a distorted shape of the spectrum. Due to this, we assign an increased uncertainty of 15 % to this measurement.

Heating effect

The longitudinal nuclear relaxation times are sensitive to the temperature. Therefore, a comparison between between $T_{\mathrm{Build\text{-}up}}$ and T_{1n} can reveal heating effects during mw irradiation. We observed differences on the order of $9\% - 20\%$ for all the investigated samples, suggesting that a temperature deviation of a few K may be present. In the case of CHCl$_3$ measured at 1.2 T, where the NMR coil spoils the homogeneity of the induced electromagnetic field, we observed deviations up to 46% between $T_{\mathrm{Build\text{-}up}}$ and T_{1n}, especially for the cases of DTBN, TL, and TN-py. Although a precise estimation of the temperature deviation is difficult without an *ad-hoc* designed study, a comparison with previous data [5] allowed us

Table S5: ^{13}C Overhauser parameter of ^{13}CHCl$_3$ for different PAs at room temperature and at 1.2 T. The leakage factor f was calculated using $T_{1n}^0 = 30$ s. [6] Errors of the concentration are $10-15\%$, for T_{1n}, $T_{\text{Build-up}}$, s, ϵ and f 10% and for ξ 15%. As $T_{1n} \neq T_{\text{Build-up}}$ for DTBN, TN-py and TL errors for ϵ and ξ are increased to 15 and 25%, respectively (see error discussion in SI sec. S2). (*) Data from ref. [5].(**) Uncertainty for this value is 15%.

^{13}C-DNP in CHCl$_3$

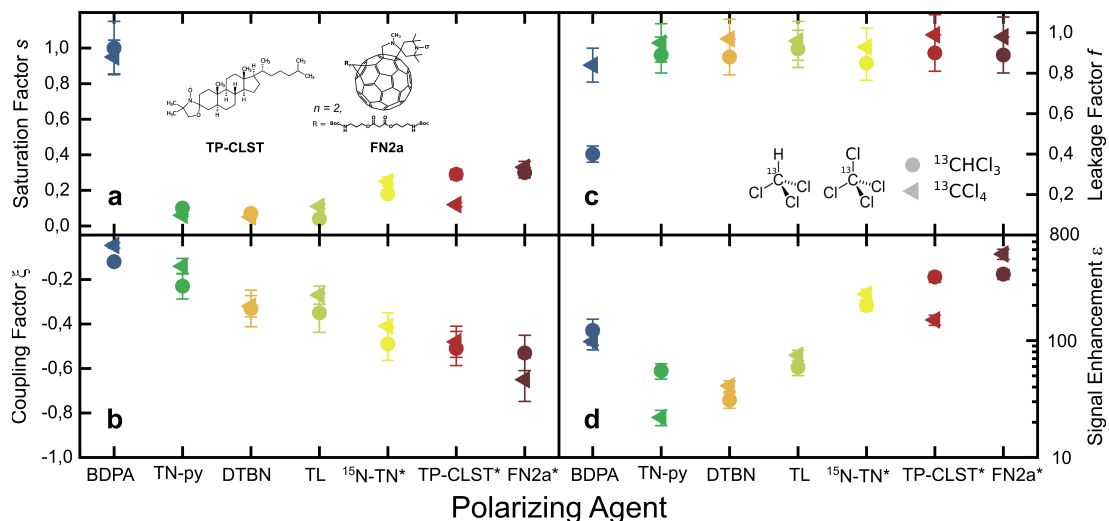|	c (mM)	T_{1n} (s)	$T_{\text{Build-up}}$ (s)	f	s_{eff}	ϵ	ξ
BDPA	10	18.1	15.4	0.40	1.00**	122	-0.12
TN-py	10	4.8	3.3	0.89	0.10	55	-0.23
DTBN	10	3.7	2.0	0.88	0.04	31	-0.33
TL	10	2.5	1.6	0.92	0.07	59	-0.35
^{15}N-TN*	10	3.9	2.9	0.85	0.18	200	-0.49
TP-CLST*	10	2.8	2.9	0.90	0.29	350	-0.51
FN2a*	4	3.5	3.1	0.89	0.30	370	-0.53

Figure S3: Plots of the ^{13}C-DNP Overhauser parameters from Tables S4 and S5. The inset displays the structure of the PAs used in ref. [5]

to estimate a maximum temperature deviation of $\sim$30 K under mw irradiation.

In terms of DNP parameters, the direct impact of a deviation in relaxation time on f is negligible, since it is mainly determined by the radical concentration. However, we expect an error on the estimation of the NMR signal enhancement.

Following these considerations, we assign an uncertainty of up to 15% for the enhancement ϵ and 25% for the coupling factor ξ for cases where $T_{\text{Build-up}}$ deviates more than 15% from T_{1n}. PA/solvent pairs, for which sample heating was observed are indicated in Tab. S1-S5.
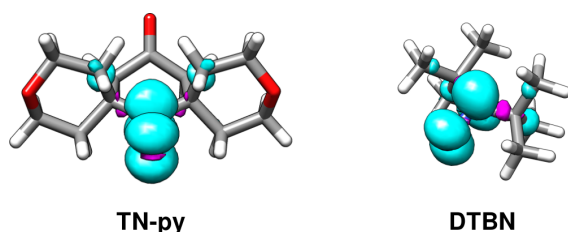
Figure S4: Electron spin density calculated for TN-py and DTBN optimized structures and represented with isosurfaces with threshold $\pm 0.002\ e/\text{Å}^3$. Color code: positive lobes in cyan, negative lobes in magenta, H white, C grey, N blue, O red.
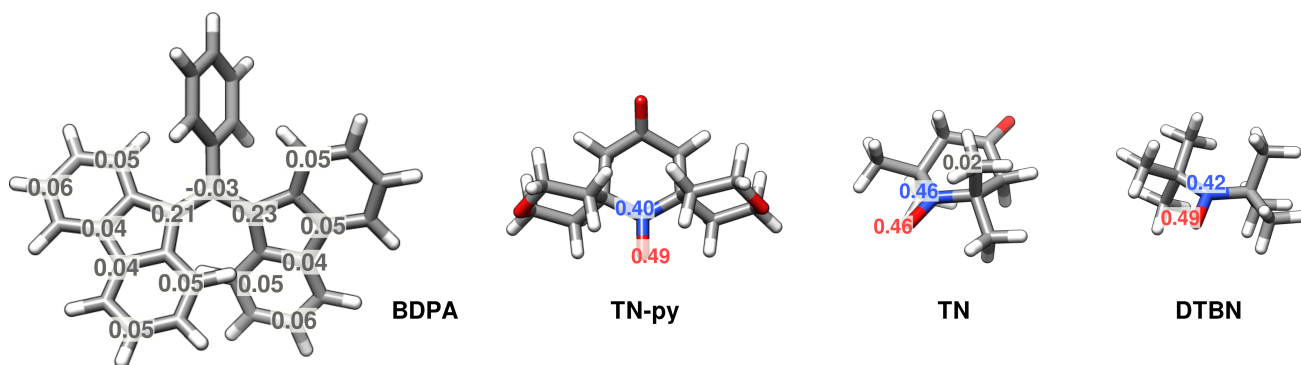

Figure S5: Optimized structures of organic radicals and Löwdin spin density shown for some of the atoms.

S3   Quantum chemistry calculations

Geometry optimizations of the radical structures (DTBN, TL, TN, TN-py) have been performed with the Orca software ver. 4.2.1. [7,8] The calculations were performed at B3LYP level of theory employing the def2-TZVPP basis set. Additionally, we employed the resolution-of-the-identity and chains-of-spheres approximations (RIJCOSX with def2/J auxiliary basis set) as well as the dispersion correction (D3BJ). Tight convergence criteria for the SCF (TIGHTSCF) and the optimization procedure (TIGHTOPT) were chosen. Spin density maps were calculated with Orca and represented with UCSF Chimera [9]: They are shown in the main text and in Figure S4. Spin populations for each atom position were obtained from the Löwdin population analysis (Figure S5).

A conformation analysis was performed for the radical TN-py (Figure S6). For estimating the relative energies of different conformers, dispersion correction energies were disregarded, as they only consider interaction within the molecule excluding the surroundings.

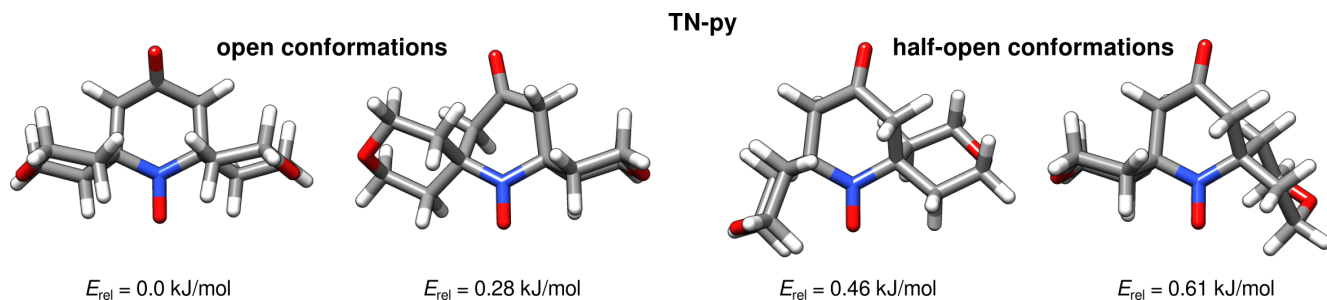Solvent-accessible surfaces (SASs) were calculated on the optimized structures of the radicals with

Figure S6: Conformations of the radical TN-py which are accessible at room temperature ($E = 2.49\ \text{kJ/mol}$ at $T = 300\ \text{K}$). An additional conformation with the piperidine arranged as a chair and the tetrahydropyrane rings in a closed conformation was calculated but it is not accessible at room temperature ($E_{\text{rel}} = 6.25\ \text{kJ/mol}$).

Table S6: SAS and SES areas calculated for the radical site of the organic radical, i.e. the NO group for NODs and the allyl group for BDPA. Values in brakets have been computed with the software Jmol, while the other calculations have been performed with UCSF Chimera.

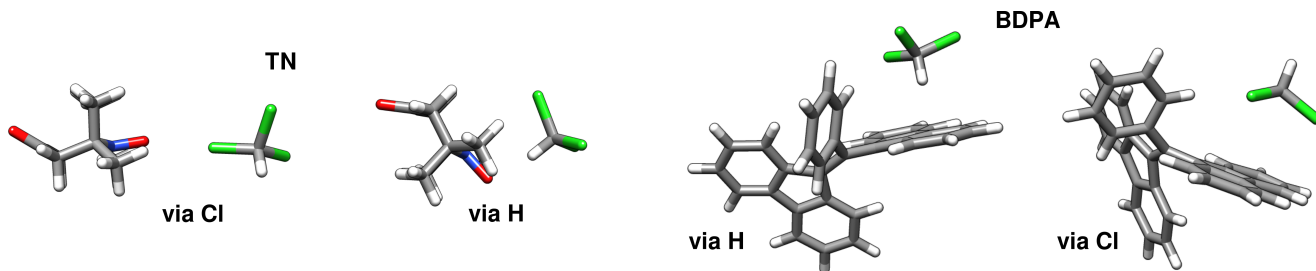| Radical	SAS (Å^2) $r_{\text{H2O}} = 1.4$ Å	SAS (Å^2) $r_{\text{CHCl3}} = 3.2$ Å	SES (Å^2) $r_{\text{H2O}} = 1.4$ Å	SES (Å^2) $r_{\text{CHCl3}} = 3.2$ Å
DTBN	23.8 [19.1]	[29.5]	13.2	11.3
TL	24.5 [20.1]	[32.9]	14.2	11.8
TN	25.6 [21.4]	[35.1]	13.4	12.0
TN-py (open)	24.7 [19.6]	[31.9]	14.2	11.5
TN-py (half-open)	15.1 [10.2]	[10.8]	11.2	8.1
FN-2a (chair)	23.7 [19.0]	[29.8]	14.1	11.5
FN-2a (boat)	28.6 [23.9]	[40.4]	14.7	13.5
BDPA	0.78 [0.07]	[0.0]	5.2	0.0

Figure S7: Optimized structures for the complexes TN/CHCl$_3$ and BDPA/CHCl$_3$. The approach "via H" and "via Cl" is shown for both radicals.

the softwares UCSF Chimera [9] and Jmol. We considered a spherical probe with a radius of 1.4 Å representing a water molecule and one with radius 3.2 Å representig CHCl$_3$. For comparison, solvent-exclusion surfaces (SESs), corresponding to the contact point between the probe sphere and the Van der Waals surface of the radical, were also calculated. The results are summarised in Table S6.

Geometry optimizations of the PA/CHCl$_3$ complexes were performed with the same functional and basis as for the radicals. In the case of BDPA and TN-py in the half-open conformation, we used geometry constrains on the radical molecule, while CHCl$_3$ was left free. The hyperfine coupling of the C atom of the CHCl$_3$ molecule was calculated with the EPR-III basis set for H, C, N, and O and IGLO-II for Cl [10]. The results for each complex are reported in Table S7, while some representative geometry optimized complexes with the approach "via H" and "via Cl" are shown in Figure S7. The energy-weighted hyperfine coupling $\langle A_{\text{FC}} \rangle$ has been calculated as described in the main text.
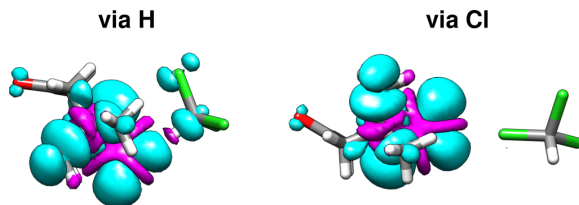

Figure S8: Geometry optimized structures of the complex TN/CHCl$_3$ for the two approaches that were considered, "via H" and "via Cl". The spin density is represented with an isosurface of 0.0002 $e/\text{Å}^3$ to highlight the spin density transfer to the C atom of the CHCl$_3$ molecule.

Table S7: Hyperfine coupling on the C atom of $CHCl_3$ calculated for the complexes $PA/CHCl_3$. The relative energy of each geometry was calculated including the dispersion correction.

DTBN/CHCl$_3$

	1	2	3	4	5
approach via	H	H	Cl	Cl	Cl
A_{FC} (MHz)	13.0	16.2	1.61	1.55	1.39
E_{rel} (kJ/mol)	0.08	0.0	20.9	158	19.9
				$\langle A_{FC}\rangle = 14.6$ MHz	

TN/CHCl$_3$

	1	2	3	4	5
approach via	H	H	Cl	Cl	
A_{FC} (MHz)	9.3	14.7	1.17	0.07	7.2
E_{rel} (kJ/mol)	2.52	0.0	15.7	8.24	4.01
				$\langle A_{FC}\rangle = 12.2$ MHz	

TL/CHCl$_3$

	1	2
approach via	H	H
A_{FC} (MHz)	10.8	12.1
E_{rel} (kJ/mol)	2.26	0.0
		$\langle A_{FC}\rangle = 11.8$ MHz

TN-py (open)/CHCl$_3$

	1	2	3	4
approach via	H	H	H	Cl
A_{FC} (MHz)	6.18	8.57	1.52	0.39
E_{rel} (kJ/mol)	0.78	0.0	9.94	13.4
			$\langle A_{FC}\rangle = 7.47$ MHz	

BDPA/CHCl$_3$

	1	2	3		
approach via	H	Cl	H/Cl	H	Cl
A_{FC} (MHz)	0.43	0.067	0.063	0.46	0.22
E_{rel} (kJ/mol)	1.89	10.6	0.0	1.31	4.85
				$\langle A_{FC}\rangle = 0.26$ MHz	

References

[1] K. Sakai, K-I. Yamada, T. Yamasaki, Y. Kinoshita, F. Mito, and H. Utsumi. Effective 2,6-substitution of piperidine nitroxyl radical by carbonyl compound. *Tetrahedron*, 66:2311–2315, 2010. Synthesis.

[2] N. Enkin, G. Liu, I. Tkach, and M. Bennati. High dnp efficiency of tempone radicals in liquid toluene at low concentrations. *Phys. Chem. Chem. Phys.*, 16:8795–8800, 2014.

[3] M-T. Tuerke and M. Bennati. Saturation factor of nitroxide radicals in liquid dnp by pulsed eldor experiments. *Phys. Chem. Chem. Phys.*, 13:3630–3633, 2011.

[4] M-T. Tuerke, G. Parigi, C. Luchinat, and M. Bennati. Overhauser dnp with [15]n labelled fremys salt at 0.35 tesla. *Phys. Chem. Chem. Phys.*, 14:502–510, 2012.

[5] M. Levien, M. Hiller, I. Tkach, M. Bennati, and T. Orlando. Nitroxide derivatives for dynamic nuclear polarization in liquids:the role of rotational diffusion. *J. Phys. Chem. Lett.*, 11:1629–1635, 2020.

[6] G. Liu, M. Levien, N. Karschin, G. Parigi, C. Luchinat, and M. Bennati. One-thousand-fold enhancement of high field liquid nuclear magnetic resonance signals at room temperature. *Nat. Chem.*, 9:676–680, feb 2017.

[7] Frank Neese. The ORCA program system. *WIREs Comput. Mol. Sci.*, 2(1):73–78, 2012.

[8] Frank Neese. Software update: the orca program system, version 4.0. *WIREs Computational Molecular Science*, 8(1):e1327, 2018.

[9] Eric F Pettersen, Thomas D Goddard, Conrad C Huang, Gregory S Couch, Daniel M Greenblatt, Elaine C Meng, and Thomas E Ferrin. UCSF Chimera—A visualization system for exploratory research and analysis. *J. Comput. Chem.*, 25(13):1605–1612, 2004.

[10] Werner Kutzelnigg, Ulrich Fleischer, and Christoph van Wüllen. Shielding calculations: Iglo method. *eMagRes*, 2007.